

Systematic investigation of π - π interactions in Near Edge X-ray

Fine Structure (NEXAFS) Spectroscopy of Paracyclophanes

Sahan D. Perera, Stephen G. Urquhart*

Department of Chemistry, University of Saskatchewan, Saskatoon, SK, Canada S7N 5C9

Abstract

NEXAFS spectroscopy has potential in the study of packing and order in organic materials, but only if intermolecular effects are understood. This work studies how π - π interactions between adjacent unsaturated groups affect their NEXAFS spectra, with a broader goal of building a general understanding of intermolecular effects in NEXAFS spectroscopy. These effects are examined using paracyclophane (PCP) molecules, in which the benzene/benzene separation distance is varied through the spacer length between benzene rings. NEXAFS spectroscopy and density functional theory (DFT) simulations are used to examine spectroscopic changes related to these π - π interactions. A characteristic red shift was observed as adjacent benzene rings get closer together. This shift is attributed to Coulombic interactions between the adjacent benzene rings, mediated through overlapping π and π^* orbitals.

* Author to whom correspondence should be addressed. E-mail: stephen.urquhart@usask.ca

1. Introduction

The near edge X-ray absorption fine structure (NEXAFS) spectra of organic molecules are predominantly sensitive to molecular bonding and orientation. As a consequence, many NEXAFS studies of organic materials focus on chemical analysis or molecular orientation, such as measurement of the presence of specific functional groups,¹⁻⁶ chemical composition in blends, alloys and composites,^{3, 7-12} or a wide range of linear dichroism measurements of molecular orientation.¹³⁻²¹

In contrast to these *intra*-molecular effects (bonding, etc.), *intermolecular* effects are not as extensively explored. These effects could be used to study molecular packing, order and disorder in molecular materials, and are therefore worthy of further study. Broadly, *intermolecular* effects in NEXAFS spectra of organic molecules are expected to arise from conformation and bonding changes (such as zwitterion formation) in the condensed state, and perturbations due to electronic interactions between adjacent molecules, such as quenching of Rydberg character in condensed phases.

Rydberg quenching has been observed in the NEXAFS spectra of simple alkanes. The spectra of small gas phase alkanes (methane, ethane, etc.) are dominated by a Rydberg series (carbon 1s \rightarrow 3s, 3p, 3d, etc.),²² but their spectra is broadened and blue-shifted in the condensed phase.²³ The origin of these differences has been controversial, but is now attributed to quenching of Rydberg character in the solid state, and the persistence of carbon 1s \rightarrow σ^* (C-H) character.²³ Quenching effects are observed in the NEXAFS spectra of saturated polymers such as polyethylene. Schöll *et al.*²⁴ demonstrated that the NEXAFS spectra of polyethylene copolymers vary with the degree of crystallinity and with disorder induced by melting, where NEXAFS features were broader in the

more disordered as well as less crystalline polymers. Recently, Schmidt *et al.*²⁵ observed Rydberg quenching in naphthalene through gas / solid comparisons and high-level DFT calculations.

Hydrogen bonding also has a role in the NEXAFS spectra of condensed species, demonstrated in the oxygen 1s spectra of water.²⁶⁻³¹

In studying the NEXAFS spectra of aromatic clusters, Rühl *et al.*³² observed a small red shift (50-70 meV) in solid clusters relative to their gas phase spectra. The magnitude of this shift was found to depend on the size and the homogeneity of the cluster.³³⁻³⁴ This effect was attributed to dynamic stabilization, in which the deformation of the core excited cluster traps the core-excited molecule in a modified geometry, where the carbon 1s $\rightarrow \pi^*$ transition will be red-shifted relative to the gas phase species.³⁴ As dynamic stabilization is proposed for clusters relative to the individual gas phase molecules,³² this effect should be constant in the solid phase, such as the PCP studies described below.

Face to face π - π interactions occur and are important for the structure and electronic property of organic electronic materials such as P3HT.³⁵⁻³⁷ Based on the potential of NEXAFS spectroscopy to see small shifts based on weak intermolecular interactions, this work explores π - π interactions between cofacial benzene rings, using paracyclophane (PCP) as a model system. PCP compounds consist of two benzene rings connected by bridging unit of variable length (see Scheme 1).³⁸⁻⁴⁰ The length of the bridging unit determines the separation between the benzene rings; shorter bridges such as in [2,2]PCP bring the benzene rings together to a distance which is lower than the limit of van der Waals interactions, and this separation between the benzene rings higher for larger bridges such as [3,3]PCP.⁴¹⁻⁴⁵

These precisely stacked π -systems held together by distinct aliphatic chains lengths, so this is a good model system to identify the role of intermolecular interactions in NEXAFS spectroscopy. Studies on direct information on π - π interactions and π orbital overlap in these materials by using NEXAFS spectroscopy are limited in literature.⁴⁰ Studies of the carbon 1s NEXAFS spectra of monolayer and multilayers of the [2,2]PCP and [4,4]PCP by Batra *et al*⁴⁰ showed an energy shift between the two species, but did not account for this in terms of π - π interactions.

In this work, π - π interactions will be examined through high-resolution carbon 1s NEXAFS spectra of PCP structures with different bridge lengths separating the facing benzene rings. These spectroscopic studies will be coupled with high quality DFT simulations of the NEXAFS spectra of these PCP models. This work will be used to examine the origin and magnitude of π - π interactions as a function of benzene / benzene separation. The knowledge of this work could be also applied to the spectroscopy of industrially important organic electronic polymers, such as P3HT, and could provide unique information on structure and order.³⁵⁻³⁷

2. Experimental

2.1. Samples and Sample Preparation

Samples: The paracyclophane (PCP) molecules used in this study are [2,2]PCP (Sigma-Aldrich 97%) and [3,3]PCP (> 95%) where [n,n] refers to the length of the alkane bridge between the benzene rings (see **Scheme 1**). [3,3]PCP was obtained from Prof. Henning Höpf (Technische Universität Braunschweig, Germany). The structures of [2,2] PCP and [3,3] PCP were verified by NMR, and used without further purification. Commercially available [5,5] PCP was found by NMR spectroscopy to not be compound claimed, and was not used in this study.

Sample Preparation: Samples were prepared by pressing the powder form onto clean indium foil (5 x 5 mm squares), and loading into a vacuum of the endstation on the SGM beamline.

2.2. NEXAFS spectroscopy

NEXAFS spectra of the [n,n] paracyclophane compounds were recorded on the SGM beamline (11ID-1) at the Canadian Light Source.⁴⁶ Spectra were recorded in Total Electron Yield (TEY) detection mode. TEY C 1s NEXAFS spectra were normalized by taking the ratio of sample current (I) and gold reference current (I_R), where the gold reference spectrum was acquired by a separate scan. To remove the normalization artifacts in the carbon 1s spectra, the intensity of the gold reference spectrum was modified such that its intensity in the pre-edge region was superimposed with the sample spectrum (I), as previously described by Otero et al.⁴⁷ Spectral analysis was performed using aXis 2000⁴⁸ and spectra were plotted for presentation using Origin 7.5. The entrance and exit slit for these measurements were 5 μ m and 3 μ m, corresponding to a resolving power greater than 5000.

The SGM monochromator energy scale was calibrated to the first CH peak in the carbon 1s NEXAFS spectra of *n*-tetracontane (*n*-C₄₀H₈₂), as previously calibrated in measurements on the Scanning Transmission X-ray Microscope on the SM beamline.⁴⁹ The calibrated energy scale was determined by measuring the spectrum of CO₂ (g) along with that of *n*-tetracontane. The carbon 1s \rightarrow 3s ($\nu=0$) and carbon 1s \rightarrow 3p ($\nu=0$) transitions in CO₂ (g) were set to 292.74 eV and 294.96 eV respectively, after the measurements of Ma *et al.*⁵⁰ On this basis, the first peak [289.15(5) eV] in the carbon 1s NEXAFS spectrum of *n*-tetracontane (*n*-C₄₀H₈₂) was calibrated to 287.48(5) eV. Measurements of *n*-tetracontane on the SGM beamline, recorded at the same time as the PCP spectra, were used to calibrate the energy scale for these spectra.

3. Computational Section

3.1 Methodology

To aid spectral assignments, DFT⁵¹⁻⁵² calculations were carried out using deMon2k package.⁵³⁻⁵⁴ NEXAFS simulations were initially performed using the transition potential (TP-DFT) method,⁵⁵⁻⁵⁶ which uses a half core hole. Subsequently, carbon 1s ionization potentials and the energy to create the lowest energy [C 1s⁻¹; π^*] core excited state were calculated with the Δ KS method.⁵⁵ This method provides more accurate energies than the Koopmans' theorem (for ionization potentials) and the transition potential (for excitation energies) approaches. Spectra obtained from TP-DFT calculations were recalibrated by setting the energy of the first transition to that calculated for the [C 1s⁻¹; π^*] core excited state by the Δ KS method.

Molecular geometries of benzene and [n,n] PCP (n = 2, 3, and 4) species were lowest energy structures, determined by ω B97X-D DFT calculations at the 6-31G* level, performed with the program Spartan' 14.⁵⁷ No imaginary frequencies were observed. For studies of benzene / benzene separation, two benzene molecules were manually placed in a cofacial structure, at different fixed benzene – benzene separation distances.

For all DFT calculations, the PBE GGA exchange and correlation functional⁵⁸⁻⁵⁹ was used, with the GEN-A4* auxiliary basis set for the core excited carbon atom, and the GEN-A2* basis set for all other atoms.⁶⁰⁻⁶¹ The orbital basis sets used are IGLO-III⁶² for the excited carbon atom, TZVP for hydrogen atoms, and effective core potentials (ECP)⁶³ for all other carbon atoms. The augmented diffuse basis set (XAS-I) was used for the core excited atom.⁵⁵ The intensity of the spectral lines is obtained from the computed dipole transition matrix elements for excitations from the core (carbon 1s) orbitals. Only the core excitation carbon 1s \rightarrow π^* transitions are considered and

simulated spectra were obtained from the DFT calculations of each non-equivalent sites by broadening the lower carbon $1s \rightarrow \pi^*$ feature as a Gaussian line. These spectra then summed according to its stoichiometric proportions to form a simulated spectrum of the π^* band.

4. Results

4.1 Carbon 1s NEXAFS Spectra of [n,n]Paracyclophanes

Figure 1 presents the experimental C 1s NEXAFS spectra for [2,2] and [3,3] paracyclophanes, recorded using TEY detection. Transition energies and assignments for the carbon $1s \rightarrow \pi^*$ band are presented in **Table 1**. The energy in the carbon $1s \rightarrow \pi^*$ region shows a red shift in the spectrum of [2,2] PCP relative to that of [3,3] PCP. At the same time, the shape of the π^* changes. The decreased alkane tether length brings the benzene rings closer together, which is correlated in a decreased carbon $1s \rightarrow \pi^*$ transition energy.

4.2 DFT simulations of the NEXAFS Spectra of [n,n] Paracyclophanes

NEXAFS simulations were obtained from Δ KS-DFT calculations of [2,2], [3,3], and [4,4] PCP, in order to interpret features observed in their experimental spectra. These simulated carbon 1s NEXAFS simulations are presented in **Figure 2**. Calculated carbon 1s ionization potentials, transition energies and, orbital term values (TV) for the lowest energy carbon $1s \rightarrow \pi^*$ transition, for the C-H and C-R sites are presented in **Table 2**.

The Δ KS-DFT simulations reproduce the trend as observed in experiment, where the carbon $1s \rightarrow \pi^*$ transition moves to lower energy as the benzene ring separation decreases, from [4,4] PCP to [2,2] PCP. The carbon $1s \rightarrow \pi^*$ transition energy shifts are larger between [4,4] PCP and [3,3] PCP than between [3,3] PCP and [2,2] PCP. The magnitude of the energy shift between [3,3] PCP

and [2,2] PCP is underestimated by the Δ KS-DFT calculations (Δ KS-DFT: 0.045 eV versus 0.2 eV in experiment). Nevertheless, the direction of the energy shift is consistent.

The calculated carbon 1s ionization potentials and the π^* orbital term values help interpret the experimental observations. The π^* orbital term values increase as the bridging group length decreases, from [4,4] PCP to [2,2] PCP. A larger term value indicates that the π^* orbital occurs at lower energy, relative to the ionization potential. In a simple molecular orbital picture, stronger bonds will have a lower energy highest occupied molecular orbital (HOMO; π) and a higher energy lowest unoccupied molecular orbital (LUMO; π^*). As the NEXAFS transitions probe the π^* LUMO, a decrease in the LUMO energy can be attributed to a weakening of the benzene ring π -bonding as the rings come closer together. The carbon 1s ionization potentials show a smaller but opposite shift, increasing between [3,3] PCP and [2,2] PCP, and shifting the core $\rightarrow \pi^*$ transition to higher energy. The term value and ionization potential shifts will partially cancel, but the overall trend remains, where core $\rightarrow \pi^*$ transition shifts to lower energy as the benzene rings move closer together.

The carbon 1s (C-R) $\rightarrow \pi^*$ transition occurs at higher energy than the carbon 1s (C-H) $\rightarrow \pi^*$ on account of the weak inductive effect of the alkyl spacer. This inductive effect increases the ionization potential (IP) of the C-R site relative to the C-H site.⁶⁴ The energy difference between the C-H and C-R carbon 1s $\rightarrow \pi^*$ transition is similar (0.24 – 0.25 eV) for [2,2] PCP and [3,3] PCP, but smaller (0.15 eV) for [4,4] PCP. This suggests that the orbital environment in [4,4] PCP is somewhat different from the two species with the rings closer together.

5. Discussion

The tether or bridging group [n,n] attached to the two benzene rings of the PCP molecule creates two non-equivalent carbon atom sites in the PCP molecule (C-H and C-R, see **Scheme 1**). A doublet structure (see **Figure 1** and **2**) arises in the carbon $1s \rightarrow \pi^*$ region from this C-H/C-R splitting. The shape of the simulation and experimental spectra differ, as experiment is further convoluted by unresolved vibronic features.⁶⁵ This π^* band shape was observed in previous NEXAFS measurements of Batra *et al.*⁴⁰ Our Δ KS calculations reproduce the experimentally observed energy shift, albeit with a different magnitude, and attribute this shift largely from changes to the energy of the π^* orbital term value with ring separation.

The benzene rings in [2,2] PCP are 3.09 Å apart.^{41-42, 45} This is significantly smaller than the van der Waals separation for the two benzene rings (e.g. two times the van der Waals radii of carbon, or 3.40 Å). The benzene/ benzene separation in [3,3] PCP is 3.30 Å,⁴³ which is slightly smaller than this van der Waals separation. Only in [4,4] PCP are the benzene rings are further apart than the van der Waals radius (3.99 Å).

The nature of the interaction between adjacent benzene rings in the PCP molecules can be examined by using molecular orbital plots of the LUMO, which are presented in **Figure 3** for the ground state and C-H / C-R core excited state LUMO in the three PCP molecules. The ground state π^* LUMO for all PCP molecules are delocalized between the top and bottom benzene rings, with an in-phase overlap of the orbitals in the space between the two benzene rings. In the MO plots of the C-H / C-R core excited states, the LUMO becomes localized onto the ring with the core hole. An orbital interaction is observed between the benzene rings in [2,2] PCP; less in [3,3] PCP, and non-existent in [4,4] PCP. The observed orbital overlap is a function of the magnitude of the

isosurface density, but the interaction is clearly greater in [2,2] PCP. The MO plots indicate that the carbon $1s \rightarrow \pi^*$ transition in PCP is sensitive to orbital interactions between the adjacent benzene rings, with a stronger interaction as the rings get closer together. Specifically, the orbital interaction is a bonding (in phase) orbital interaction between the rings, and an antibonding (π^*) within each ring. This interaction will scale with the closeness of the benzene rings.

Another way to investigate the shift in carbon $1s \rightarrow \pi^*$ transition energy with benzene – benzene separation is to use a dibenzene model with different separation distances. **Figure 4** presents a plot of the lowest energy carbon $1s \rightarrow \pi^*$ transition energy (Δ KS DFT) for this dibenzene species as a function of inter-ring distance, from 2.6 Å - 4.0 Å. This plot shows a clear red shift as the rings get closer together, with a larger slope below the van der Waals separation distance (3.4 Å). As the separation increases, the carbon $1s \rightarrow \pi^*$ transition energy increases and tends to an asymptote. This indicates a relatively long range effect on the carbon $1s \rightarrow \pi^*$ transition energy, with a larger shift below near the van der Waals separation distance.

6. Conclusions

The carbon $1s$ NEXAFS spectroscopy of [2,2] PCP and [3,3] PCP have been recorded and interpreted with the aid of DFT calculations. PCP compounds are used to provide a careful examination of π - π interactions, as they provide an experiment model defined benzene-benzene separation distances. The systematic spectral trend in the carbon $1s \rightarrow \pi^*$ transition energies was explored as a function of benzene-benzene separation distances. These observed trends of the were interpreted with Δ KS-DFT calculations. Variations in both core binding and π^* orbital energies arose from magnitude of π - π interactions, which increase for PCP molecules with a smaller bridging unit.

The knowledge of this work can be used to simply and understand the spectroscopy of complex organic electronic polymers, and could provide unique information on structure and order.

ACKNOWLEDGMENTS

SGU is supported by NSERC (Canada) and Canadian Foundation for Innovation. NEXAFS studies were performed at the Spherical Grating Monochromator (SGM, 11ID-1) and the Spectromicroscopy (SM; 10ID-1) beamlines at the Canadian Light Source (CLS). NMR studies were performed at the Saskatchewan Structural Sciences Centre (SSSC). The CLS is supported by the Natural Sciences and Engineering Research Council of Canada, the National Research Council Canada, the Canadian Institutes of Health Research, the Province of Saskatchewan, Western Economic Diversification Canada, and the University of Saskatchewan. The SSSC is supported by the Canada Foundation for Innovation, Natural Sciences and Engineering Research Council of Canada, the Department of Chemistry and the University of Saskatchewan.

Table 1: Experimental Carbon 1s $\rightarrow \pi^*$ Transition Energies from the NEXAFS Spectra of [2,2] and [3,3] PCPs.

[n,n]PCP	Carbon 1s $\rightarrow \pi^*$ Transition Energy (eV)	
	C-H site	C-R site
[2,2]PCP	284.8	284.9
[3,3]PCP	285.0	285.3

Table 2: The Calculated ionization potential, transition energies, and term values of [2,2], [3,3] and [4,4] PCP from the $\Delta(KS)$ method.

[n,n]PCP	Ionization Potential (eV)		Carbon 1s \rightarrow π^* Transition Energy (eV)		π^* Orbital Term value (eV)	
	C-H site (eV)	C-R site (eV)	C-H site (eV)	C-R site (eV)	C-H site (eV)	C-R site (eV)
[2,2] PCP	288.772	288.891	284.087	284.328	4.685	4.563
[3,3] PCP	288.644	288.798	284.132	284.390	4.512	4.408
[4,4] PCP	288.732	288.847	284.382	284.532	4.350	4.315

Figure captions

Scheme 1: Chemical structures of [2,2]paracyclophane and [3,3]paracyclophane.

Figure 1: Carbon 1s NEXAFS spectra of [2,2] and [3,3] paracyclophane, recorded with total electron yield (TEY) detection.

Figure 2: Δ (KS) DFT simulations of the NEXAFS spectra of [2,2], [3,3] and [4,4] paracyclophane.

Figure 3 (a-c) Iso-surface plots of the LUMOs for [2,2]PCP, [3,3]PCP and [4,4]PCP, respectively, from ground state DFT calculations. (d-f) Iso-surface plots of the core excited state LUMOs for [2,2]PCP, [3,3]PCP and [4,4]PCP, respectively, from DFT calculations. The Iso-surface value for all the plots set to 0.03.

Figure 4 Variation in the calculated carbon 1s $\rightarrow \pi^*$ transition energy in dibenzene molecule as a function of inter-ring distance. Energies were calculated by the Δ (KS) DFT method.

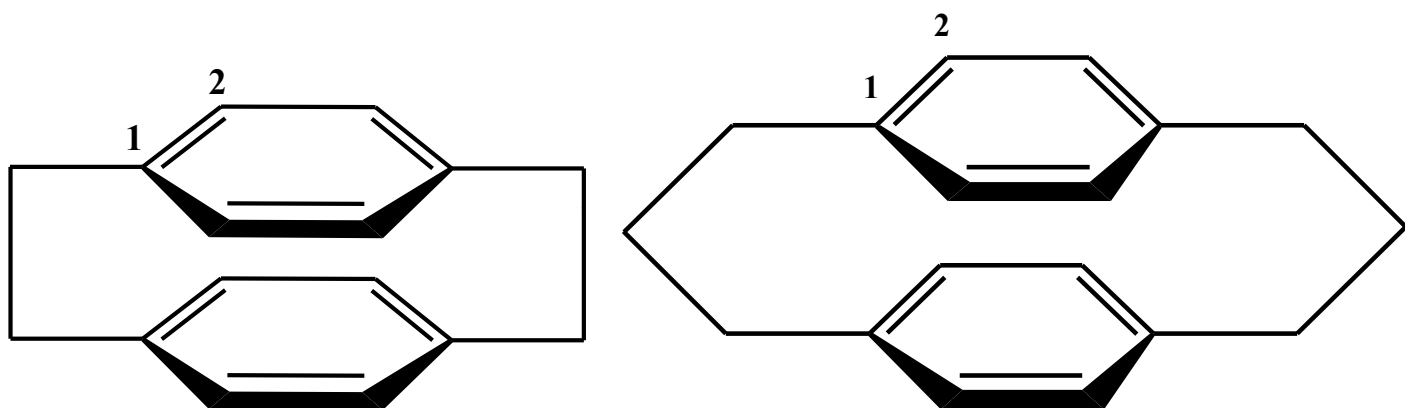
References

1. Dhez, O.; Ade, H.; Urquhart, S. G., Calibrated Nexafs Spectra of Some Common Polymers. *Journal of Electron Spectroscopy and Related Phenomena* **2003**, *128*, 85-96.
2. Urquhart, S., Nexafs Spectroscopy and Microscopy of Natural and Synthetic Polymers. *Chemical Applications of Synchrotron Radiation* **2002**, 285.
3. Rightor, E. G.; Urquhart, S. G.; Hitchcock, A. P.; Ade, H.; Smith, A. P.; Mitchell, G. E.; Priester, R. D.; Aneja, A.; Appel, G.; Wilkes, G., Identification and Quantitation of Urea Precipitates in Flexible Polyurethane Foam Formulations by X-Ray Spectromicroscopy. *Macromolecules* **2002**, *35*, 5873-5882.
4. Singh, B.; Fang, Y.; Cowie, B. C. C.; Thomsen, L., Nexafs and Xps Characterisation of Carbon Functional Groups of Fresh and Aged Biochars. *Organic Geochemistry*, *77*, 1-10.
5. Gainar, A.; Stevens, J. S.; Jaye, C.; Fischer, D. A.; Schroeder, S. L. M., Nexafs Sensitivity to Bond Lengths in Complex Molecular Materials: A Study of Crystalline Saccharides. *The Journal of Physical Chemistry B*, *119*, 14373-14381.
6. Heymann, K.; Lehmann, J.; Solomon, D.; Schmidt, M. W. I.; Regier, T., C 1s K-Edge near Edge X-Ray Absorption Fine Structure (Nexafs) Spectroscopy for Characterizing Functional Group Chemistry of Black Carbon. *Organic Geochemistry*, *42*, 1055-1064.
7. Lipton-Duffin, J.; Miwa, J. A.; Urquhart, S. G.; Contini, G.; Cossaro, A.; Casalis, L.; Barth, J. V.; Floreano, L.; Morgante, A.; Rosei, F., Binding Geometry of Hydrogen-Bonded Chain Motif in Self-Assembled Gratings and Layers on Ag(111). *Langmuir* **2012**, *28*, 14291-14300.
8. Qaqish, S. E.; Urquhart, S. G.; Lanke, U.; Brunet, S. M. K.; Paige, M. F., Phase Separation of Palmitic Acid and Perfluorooctadecanoic Acid in Mixed Langmuir-Blodgett Monolayer Films. *Langmuir* **2009**, *25*, 7401-7409.
9. Iyer, G. R. S.; Wang, J.; Wells, G.; Bradley, M. P.; Borondics, F., Nanoscale Imaging of Freestanding Nitrogen Doped Single Layer Graphene. *Nanoscale* **2015**, *7*, 2289-2294.
10. Hitchcock, A. P.; Berejnov, V.; Lee, V.; West, M.; Colbow, V.; Dutta, M.; Wessel, S., Carbon Corrosion of Proton Exchange Membrane Fuel Cell Catalyst Layers Studied by Scanning Transmission X-Ray Microscopy. *Journal of Power Sources* **2014**, *266*, 66-78.
11. Meier, R.; Schindler, M.; Muller-Buschbaum, P.; Watts, B., Residual Solvent Content in Conducting Polymer-Blend Films Mapped with Scanning Transmission X-Ray Microscopy. *Physical Review B*, *84*, 174205/1-174205/6.
12. Zhong, J.; Zhang, H.; Sun, X.; Lee, S. T., Synchrotron Soft X-Ray Absorption Spectroscopy Study of Carbon and Silicon Nanostructures for Energy Applications. *Advanced Materials*, *26*, 7786-7806.
13. Ney, A.; Ney, V.; Ollefs, K.; Schauries, D.; Wilhelm, F.; Rogalev, A., X-Ray Linear Dichroism: An Element-Selective Spectroscopic Probe for Local Structural Properties and Valence. *Journal of Surfaces and Interfaces of Materials*, *2*, 14-23.
14. Rossi, G.; d'Acapito, F.; Amidani, L.; Boscherini, F.; Pedio, M., Local Environment of Metal Ions in Phthalocyanines: K-Edge X-Ray Absorption Spectra. *Physical Chemistry Chemical Physics*, *18*, 23686-23694.
15. Marchetto, H.; Schmidt, T.; Groh, U.; Maier, F. C.; Levesque, P. L.; Fink, R. H.; Freund, H.-J.; Umbach, E., Direct Observation of Epitaxial Organic Film Growth: Temperature-Dependent Growth Mechanisms and Metastability. *Physical Chemistry Chemical Physics*, *17*, 29150-29160.
16. Baio, J. E.; Jaye, C.; Fischer, D. A.; Weidner, T., High-Throughput Analysis of Molecular Orientation on Surfaces by Nexafs Imaging of Curved Sample Arrays. *ACS Combinatorial Science*, *16*, 449-453.
17. Patel, S. N.; Su, G. M.; Luo, C.; Wang, M.; Perez, L. A.; Fischer, D. A.; Prendergast, D.; Bazan, G. C.; Heeger, A. J.; Chabiniy, M. L., Nexafs Spectroscopy Reveals the Molecular Orientation in Blade-Coated Pyridal [2, 1, 3] Thiadiazole-Containing Conjugated Polymer Thin Films. *Macromolecules*, *48*, 6606-6616.

18. Masnadi, M.; Urquhart, S. G., Indirect Molecular Epitaxy: Deposition of N-Alkane Thin Films on Au Coated NaCl (001) and HcpG (0001) Surfaces. *Langmuir*, **29**, 6302-6307.
19. Urquhart, S. G.; Lanke, U. D.; Fu, J., Characterisation of Molecular Orientation in Organic Nanomaterials by X-Ray Linear Dichroism Microscopy. *International Journal of Nanotechnology* **2008**, *5*, 1138-1170.
20. Fu, J.; Urquhart, S. G., Linear Dichroism in the X-Ray Absorption Spectra of Linear N-Alkanes. *The Journal of Physical Chemistry A* **2005**, *109*, 11724-11732.
21. Ade, H., Nexafs and X-Ray Linear Dichroism Microscopy and Applications to Polymer Science. In *X-Ray Microscopy and Spectromicroscopy: Status Report from the Fifth International Conference, Würzburg, August 19–23, 1996*, Thieme, J.; Schmahl, G.; Rudolph, D.; Umbach, E., Eds. Springer Berlin Heidelberg: Berlin, Heidelberg, 1998; pp 219-229.
22. Urquhart, S. G.; Gillies, R., Rydberg–Valence Mixing in the Carbon 1s near-Edge X-Ray Absorption Fine Structure Spectra of Gaseous Alkanes. *The Journal of Physical Chemistry A* **2005**, *109*, 2151-2159.
23. Urquhart, S. G.; Gillies, R., Matrix Effects in the Carbon 1s near Edge X-Ray Absorption Fine Structure Spectra of Condensed Alkanes. *The Journal of Chemical Physics* **2006**, *124*, 234704.
24. Scholl, A.; Fink, R.; Umbach, E.; Mitchell, G. E.; Urquhart, S. G.; Ade, H., Towards a Detailed Understanding of the Nexafs Spectra of Bulk Polyethylene Copolymers and Related Alkanes. *Chemical Physics Letters* **2003**, *370*, 834-841.
25. Schmidt, N.; Wenzel, J.; Dreuw, A.; Fink, R. H.; Hieringer, W., Matrix Effects in the C 1s Photoabsorption Spectra of Condensed Naphthalene. *The Journal of Chemical Physics*, *145*, 234307.
26. Nilsson, A.; Pettersson, L. G. M., The Structural Origin of Anomalous Properties of Liquid Water. *Nature communications*, *6*.
27. Fransson, T.; Zhovtobriukh, I.; Coriani, S.; Wikfeldt, K. T.; Norman, P.; Pettersson, L. G. M., Requirements of First-Principles Calculations of X-Ray Absorption Spectra of Liquid Water. *Physical Chemistry Chemical Physics*, *18*, 566-583.
28. Wernet, P.; Nordlund, D.; Bergmann, U.; Cavalleri, M.; Odelius, M.; Ogasawara, H.; Näslund, L.; Hirsch, T. K.; Ojamäe, L.; Glatzel, P., The Structure of the First Coordination Shell in Liquid Water. *Science* **2004**, *304*, 995-999.
29. Prendergast, D.; Galli, G., X-Ray Absorption Spectra of Water from First Principles Calculations. *Physical Review Letters* **2006**, *96*, 215502.
30. Cai, Y. Q.; Mao, H. K.; Chow, P. C.; Tse, J. S.; Ma, Y.; Patchkovskii, S.; Shu, J. F.; Struzhkin, V.; Hemley, R. J.; Ishii, H., Ordering of Hydrogen Bonds in High-Pressure Low-Temperature H₂O. *Physical Review Letters* **2005**, *94*, 025502.
31. Leetmaa, M.; Ljungberg, M. P.; Lyubartsev, A.; Nilsson, A.; Pettersson, L. G. M., Theoretical Approximations to X-Ray Absorption Spectroscopy of Liquid Water and Ice. *Journal of Electron Spectroscopy and Related Phenomena* **2010**, *177*, 135-157.
32. Bradeanu, I. L.; Flesch, R.; Kosugi, N.; Pavlychev, A. A.; Ruhl, E., C 1s → π* Excitation in Variable Size Benzene Clusters. *Physical Chemistry Chemical Physics* **2006**, *8*, 1906-1913.
33. Flesch, R.; Pavlychev, A. A.; Neville, J. J.; Blumberg, J.; Kuhlmann, M.; Tappe, W.; Senf, F.; Schwarzkopf, O.; Hitchcock, A. P.; Ruhl, E., Dynamic Stabilization in Excited Nitrogen Clusters. *Physical Review Letters* **2001**, *86*, 3767.
34. Pavlychev, A. A.; Flesch, R.; Ruhl, E., Line Shapes of Excited Molecular Clusters. *Physical Review A* **2004**, *70*, 015201.
35. Kim, D. H.; Park, Y. D.; Jang, Y.; Yang, H.; Kim, Y. H.; Han, J. I.; Moon, D. G.; Park, S.; Chang, T.; Chang, C., Enhancement of Field Effect Mobility Due to Surface-Mediated Molecular Ordering in Regioregular Polythiophene Thin Film Transistors. *Advanced Functional Materials* **2005**, *15*, 77-82.

36. Obata, S.; Shimoi, Y., Control of Molecular Orientations of Poly(3-Hexylthiophene) on Self-Assembled Monolayers: Molecular Dynamics Simulations. *Physical Chemistry Chemical Physics*, **15**, 9265-9270.
37. Seok, J.; Balik, C. M.; Ade, H. In *Improved Crystalline Orientation of Poly (3-Hexyl Thiophene) in Bulk Hetero-Junction Polymer Solar Cells*, 240th ACS National Meeting and Exposition.
38. Hu, W.; Gompf, B.; Pflaum, J.; Schweitzer, D.; Dressel, M., Transport Properties of [2, 2]-Paracyclophane Thin Films. *Applied Physics Letters* **2004**, *84*, 4720-4722.
39. Bachrach, S. M., Dft Study of [2.2]-, [3.3]-, and [4.4] Paracyclophanes: Strain Energy, Conformations, and Rotational Barriers. *The Journal of Physical Chemistry A*, **115**, 2396-2401.
40. Batra, A.; Kladnik, G.; Vazquez, H.; Meisner, J. S.; Floreano, L.; Nuckolls, C.; Cvetko, D.; Morgante, A.; Venkataraman, L., Quantifying through-Space Charge Transfer Dynamics in Pi-Coupled Molecular Systems. *Nature Communications*, **3**, 1086.
41. Hope, H.; Bernstein, J.; Trueblood, K. N., The Crystal and Molecular Structure of 1, 1, 2, 2, 9, 9, 10, 10-Octafluoro-[2, 2] Paracyclophane and a Reinvestigation of the Structure of [2, 2] Paracyclophane. *Acta Crystallographica Section B: Structural Crystallography and Crystal Chemistry* **1972**, *28*, 1733-1743.
42. Lonsdale, D. K.; Milledge, H. J.; Rao, K. V. K. In *Studies of the Structure, Thermal Expansion and Molecular Vibrations of Di-P-Xylylene*, Proceedings of the Royal Society of London A: Mathematical, Physical and Engineering Sciences, The Royal Society: 1960; pp 82-100.
43. Gantzel, P. K.; Trueblood, K. N., The Crystal and Molecular Structure of [3.3] Paracyclophane. *Acta Crystallographica* **1965**, *18*, 958-968.
44. Lyssenko, K. A.; Korlyukov, A. A.; Antipin, M. Y., The Role of Intermolecular H... H and C ... H Interactions in the Ordering of [2.2] Paracyclophane at 100 K: Estimation of the Sublimation Energy from the Experimental Electron Density Function. *Mendeleev Communications* **2005**, *15*, 90-92.
45. Brown, C. J.; Farthing, A. C., Preparation and Structure of Di-P-Xylylene. *Nature* **1949**, *164*, 915-916.
46. Regier, T.; Krochak, J.; Sham, T. K.; Hu, Y. F.; Thompson, J.; Blyth, R. I. R., Performance and Capabilities of the Canadian Dragon: The Sgm Beamline at the Canadian Light Source. *Nuclear Instruments and Methods in Physics Research Section A: Accelerators, Spectrometers, Detectors and Associated Equipment* **2007**, *582*, 93-95.
47. Otero, E.; Wilks, R. G.; Regier, T.; Blyth, R. I. R.; Moewes, A.; Urquhart, S. G., Substituent Effects in the Iron 2p and Carbon 1s Edge near-Edge X-Ray Absorption Fine Structure (Nexafs) Spectroscopy of Ferrocene Compounds. *The Journal of Physical Chemistry A* **2008**, *112*, 624-634.
48. Hitchcock, A. P. *Axis2000*, 2017.
49. Kaznatcheev, K. V.; Karunakaran, C.; Lanke, U. D.; Urquhart, S. G.; Obst, M.; Hitchcock, A. P., Soft X-Ray Spectromicroscopy Beamline at the Cls: Commissioning Results. *Nuclear Instruments and Methods in Physics Research Section A: Accelerators, Spectrometers, Detectors and Associated Equipment* **2007**, *582*, 96-99.
50. Ma, Y.; Chen, C. T.; Meigs, G.; Randall, K.; Sette, F., High-Resolution K-Shell Photoabsorption Measurements of Simple Molecules. *Physical Review A* **1991**, *44*, 1848.
51. Kohn, W.; Sham, L. J., Self-Consistent Equations Including Exchange and Correlation Effects. *Physical Review* **1965**, *140*, A1133.
52. Hohenberg, P.; Kohn, W., Inhomogeneous Electron Gas. *Physical Review* **1964**, *136*, B864.
53. Geudtner, G., et al., Demon2k. *Wiley Interdisciplinary Reviews: Computational Molecular Science* **2012**, *2*, 548-555.
54. Koster, A. M.; Geudtner, G.; Calaminici, P.; Casida, M. E.; Dominguez, V. D.; Flores-Moreno, R.; Gamboa, G. U.; Goursot, A.; Heine, T.; Ipatov, A. *Demon2k, Version 3; the Demon Developers, Cinvestav: Mexico City, 2011.*

55. Triguero, L.; Pettersson, L. G. M.; Ågren, H., Calculations of near-Edge X-Ray-Absorption Spectra of Gas-Phase and Chemisorbed Molecules by Means of Density-Functional and Transition-Potential Theory. *Physical Review B* **1998**, *58*, 8097.
56. Leetmaa, M.; Ljungberg, M.; Nilsson, A.; Pettersson, L. G. M., *X-Ray Spectroscopy Calculations within Kohn–Sham Dft: Theory and Applications*; Wiley-VCH Verlag GmbH & Co. : Weinheim, Germany, 2009, p 221-264.
57. *Spartan' 14*, Wavefunction Inc.: Irvine, CA.
58. Perdew, J. P.; Burke, K.; Ernzerhof, M., Generalized Gradient Approximation Made Simple. *Physical Review Letters* **1996**, *77*, 3865.
59. Hammer, B.; Hansen, L. B.; Narskov, J. K., Improved Adsorption Energetics within Density-Functional Theory Using Revised Perdew-Burke-Ernzerhof Functionals. *Physical Review B* **1999**, *59*, 7413.
60. Calaminici, P.; Janetzko, F.; Kaster, A. M.; Mejia-Olvera, R.; Zuniga-Gutierrez, B., Density Functional Theory Optimized Basis Sets for Gradient Corrected Functionals: 3 D Transition Metal Systems. *The Journal of Chemical Physics* **2007**, *126*, 044108.
61. Calaminici, P.; Flores-Moreno, R.; Koester, A. M., A Density Functional Study of Structures and Vibrations of Ta₃O and Ta₃O. *Computing Letters* **2005**, *1*, 164-171.
62. Kutzelnigg, W.; Fleischer, U.; Schindler, M., The Iqlo-Method: Ab-Initio Calculation and Interpretation of Nmr Chemical Shifts and Magnetic Susceptibilities. In *Deuterium and Shift Calculation*, Springer: 1990; pp 165-262.
63. Pettersson, L. G. M.; Wahlgren, U.; Gropen, O., Effective Core Potential Parameters for First and Second Row Atoms. *The Journal of Chemical Physics* **1987**, *86*, 2176-2184.
64. Cooney, R. R.; Urquhart, S. G., Chemical Trends in the near-Edge X-Ray Absorption Fine Structure of Monosubstituted and Para-Bisubstituted Benzenes. *The Journal of Physical Chemistry B* **2004**, *108*, 18185-18191.
65. Urquhart, S. G.; Ade, H.; Rafailovich, M.; Sokolov, J. S.; Zhang, Y., Chemical and Vibronic Effects in the High-Resolution near-Edge X-Ray Absorption Fine Structure Spectra of Polystyrene Isotopomers. *Chemical Physics Letters* **2000**, *322*, 412-418.



Scheme 1

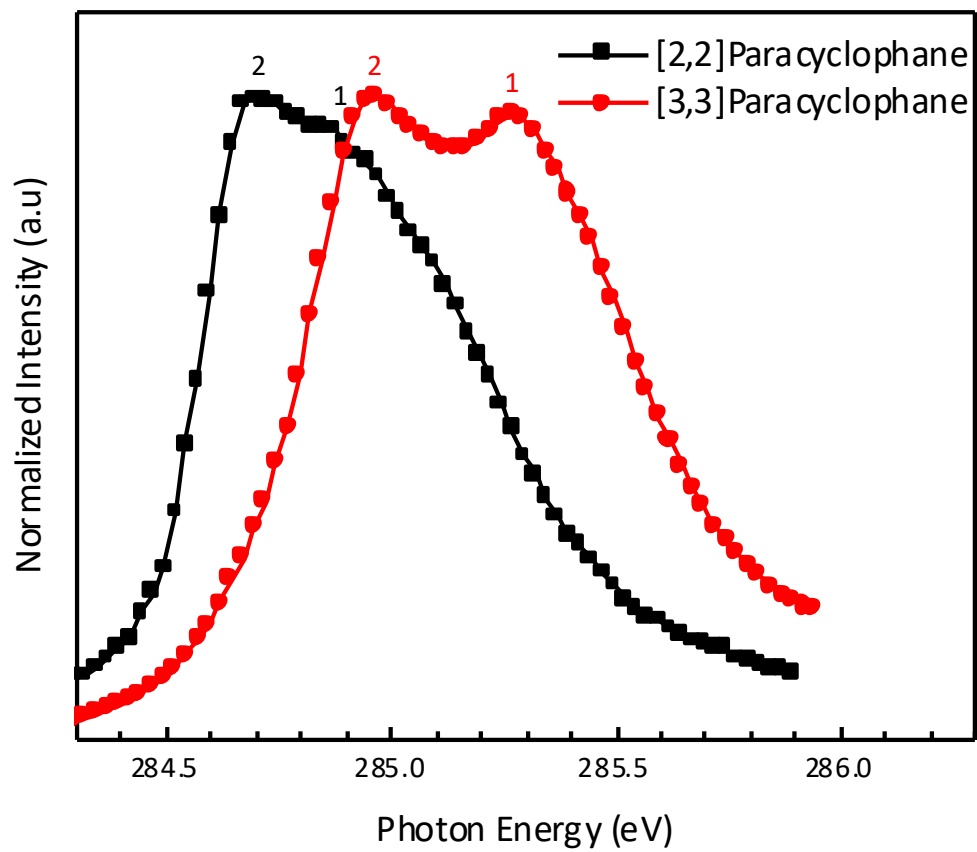


Figure 1:

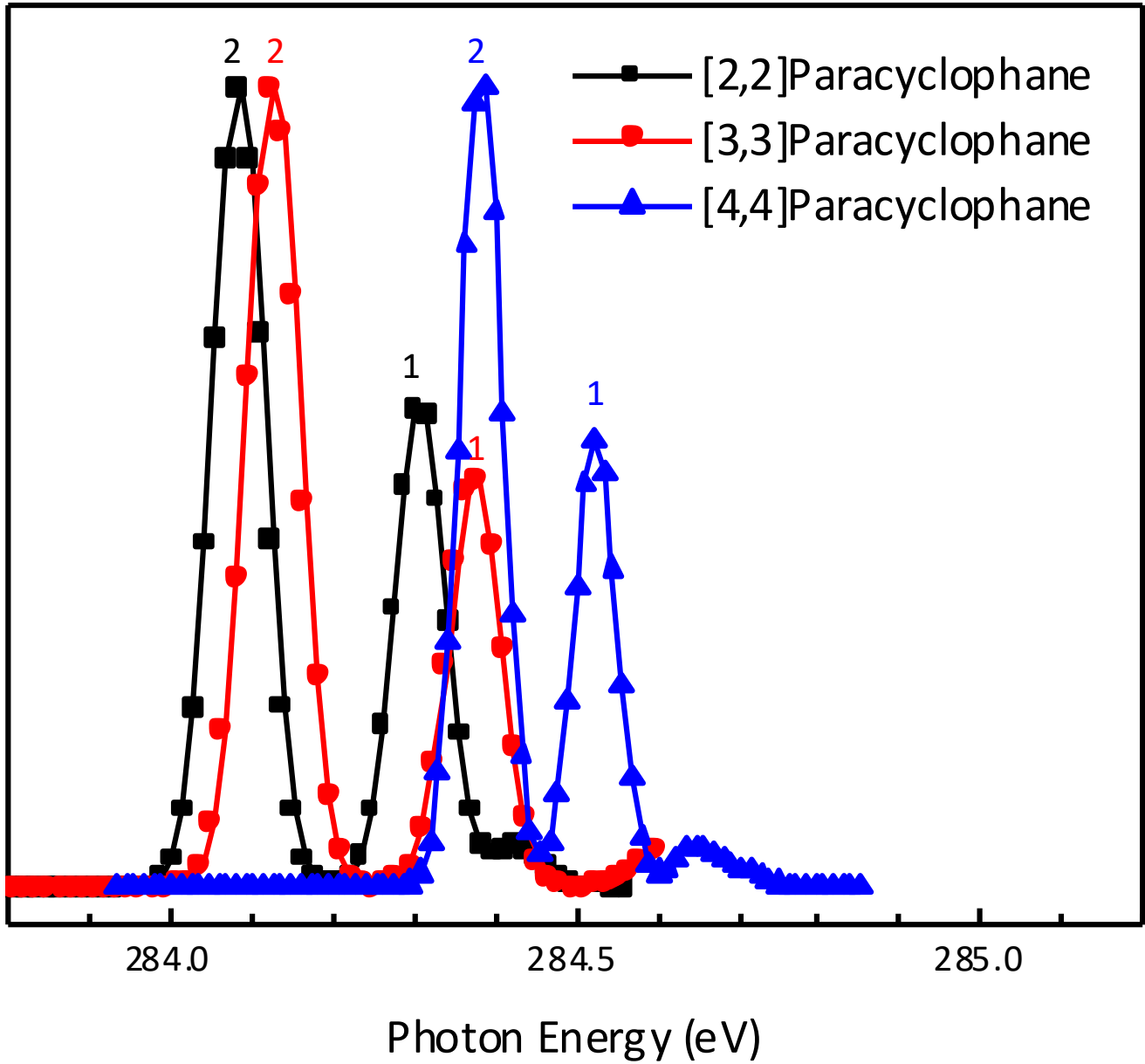


Figure 2:

QUESTION: why does the trace of 3,3 and 2,2 cut off at low energy

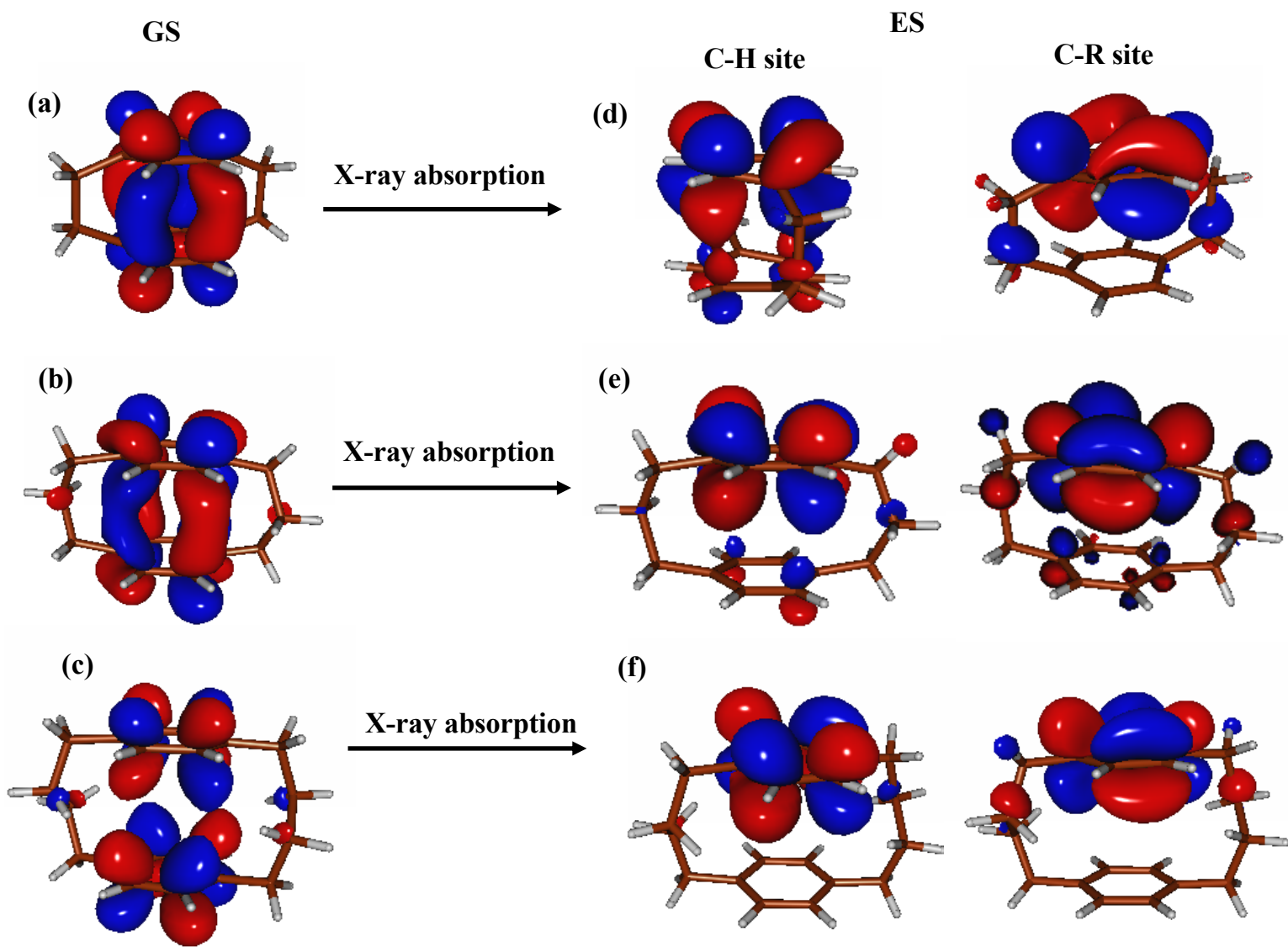


Figure 3:

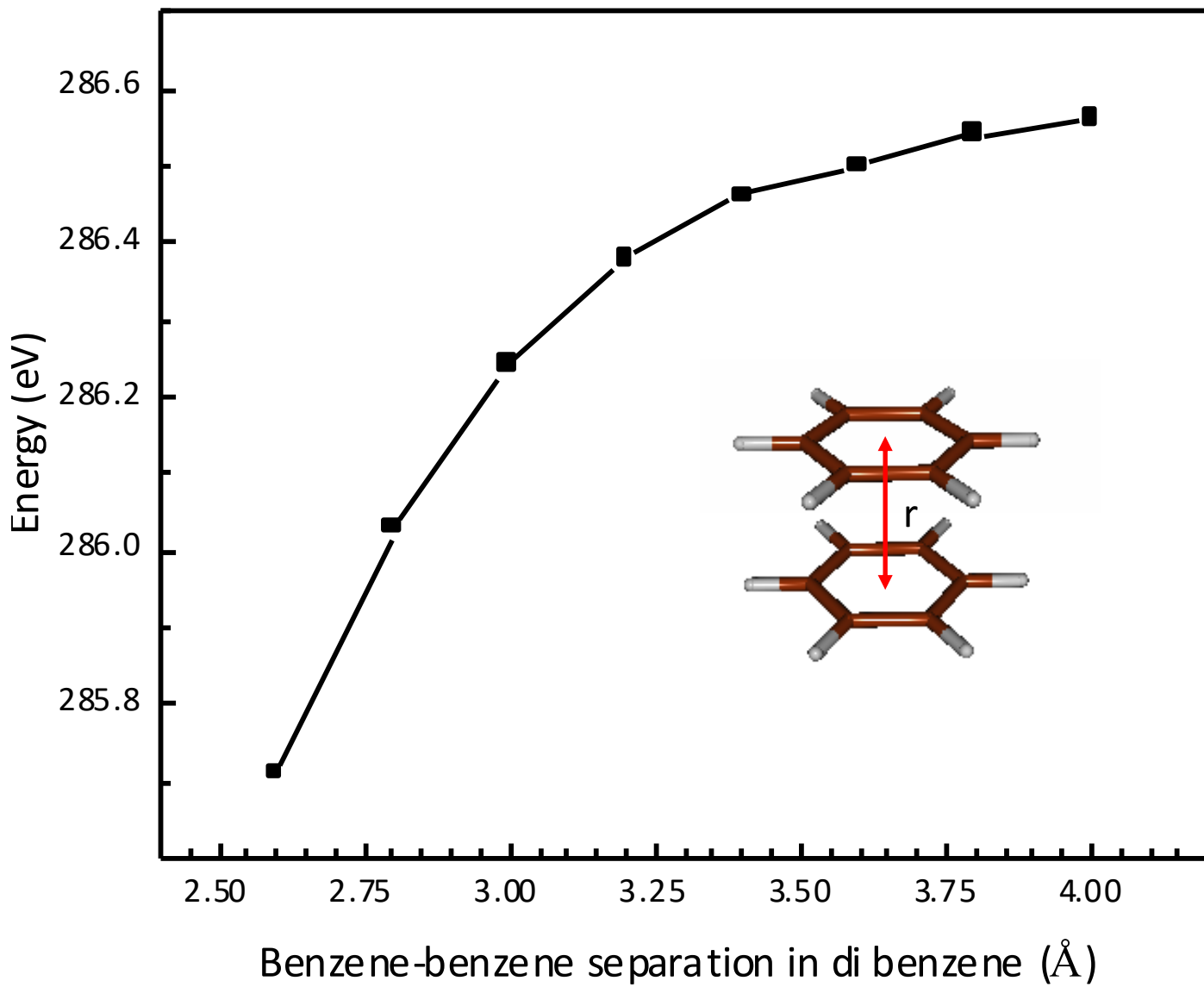


Figure 4:

Table S1 Calculated ionization potential, transition energies, and term values of [2,2], [3,3] and [4,4] PCPs, from TP-DFT calculations.

[n,n]PCP	Ionization Potential (eV)		Carbon 1s \rightarrow π^* Transition Energy (eV)		π^* Orbital Term value ^a (eV)	
	C-H site	C-R site	C-H site	C-R site	C-H site	C-R site
[2,2] PCP	290.363	290.529	286.232	286.556	4.131	3.973
[3,3] PCP	290.241	290.439	286.293	286.624	3.948	3.815
[4,4] PCP	290.325	290.480	286.550	286.793	3.774	3.687

a.) Transition energy = Energy of the core hole orbital (Ionization potential) – energy of the lowest unoccupied molecular orbital (Term value)

Table S2: Calculated ionization potential, transition energies, and term values of dibenzene with different benzene-benzene separation from TP-DFT calculations for carbon 1s \rightarrow π^* transition (C-H site).

Dibenzene molecule with different benzene-benzene separations (Å)	Ionization Potential (eV)	Carbon 1s \rightarrow π^* Transition Energy (eV)	π^* Orbital Term value ^a (eV)
2.6	290.382	285.718	4.664
2.8	290.488	286.036	4.452
3.0	290.562	286.240	4.316
3.2	290.616	289.377	4.239
3.4	290.660	286.449	4.201
3.6	290.695	286.507	4.188
3.8	290.722	286.532	4.190
4.0	290.747	286.548	4.199

a.) Transition energy = Energy of the core hole orbital (Ionization potential) – energy of the lowest unoccupied molecular orbital (Term value)

Table S3: Calculated ionization potential, transition energies, and term values of dibenzene with different benzene-benzene separation from $\Delta(KS)$ method for carbon $1s \rightarrow \pi^*$ transition (C-H site).

Dibenzene molecule with different benzene-benzene separations (Å)	Ionization Potential (eV)	Carbon $1s \rightarrow \pi^*$ Transition Energy (eV)	π^* Orbital Term value (eV)
2.6	288.742	283.594	5.147
2.8	288.855	283.862	4.993
3.0	288.934	284.036	4.898
3.2	288.993	284.147	4.846
3.4	289.038	284.217	4.821
3.6	289.074	284.260	4.814
3.8	289.104	284.286	4.818
4.0	289.130	284.303	4.827